Detecting Regime Transitions in Slurry Bubble Columns using Pressure Time Series

Keshav C. Ruthiya, Vinit P. Chilekar, Maurice J. F. Warnier, John van der Schaaf, Ben F. M. Kuster, and Jaap C. Schouten
Laboratory of Chemical Reactor Engineering, Dept. of Chemical Engineering and Chemistry, Eindhoven University of Technology, P.O. Box 513, 5600 MB Eindhoven, The Netherlands

J. Ruud van Ommen
Reactor and Catalysis Engineering, Dept. of Chemical Technology, Delft University of Technology, Julianalaan 136, 2628 BL Delft, The Netherlands

DOI 10.1002/aic.10474
Published online May 10, 2005 in Wiley InterScience (www.interscience.wiley.com).

Changes in the coherent standard deviation and in the average frequency of measured pressure time series with gas velocity, are proposed, as unique and unambiguous criteria to mark flow regime transitions in slurry bubble columns. In a 2-dimensional (2-D) slurry bubble column, pressure time series are measured at different gas velocities simultaneously with high-speed video recording of the gas-liquid flow. The frequency of occurrence and the average diameter of the large bubbles are determined from video image analysis. The gas velocity where the first large bubbles are detected, with an average diameter of 1.5 cm, and with a frequency of occurrence of one bubble per s, is designated as the first regime transition point (transition from the homogeneous regime to the transition regime). At this point, the coherent standard deviation of the measured pressure fluctuations clearly increases from zero. The gas velocity where the average diameter and the frequency of occurrence of the large bubbles become constant, is designated as the second regime transition point (transition from the transition regime to the heterogeneous regime). From this point onward, the slope of the coherent standard deviation of the measured pressure fluctuations clearly decreases with gas velocity, while the average frequency becomes constant. These clear changes with gas velocity in the coherent standard deviation, and in the average frequency are also demonstrated in a 3-D slurry bubble column. © 2005 American Institute of Chemical Engineers *AIChE J,* 51: 1951–1965, 2005
Keywords: slurry bubble column, regime transition, imaging, pressure fluctuations, average frequency, coherent standard deviation.

Introduction

Proper design and scale-up of slurry bubble columns largely depend on the accurate prediction of the gas holdup. For example, mass and heat transfer depend strongly on the (local) fluid dynamics and are mostly quantified through correlations in which the gas holdup plays an important role. It is well-known that the gas holdup in slurry bubble columns depends on the gas velocity, and many quantitative correlations can be found in literature.[1-4] Some of these gas holdup vs. gas velocity correlations contain a transitional gas holdup (ε_{trans}) at a corresponding transition gas velocity (u_{trans}) to properly describe the dependence of gas holdup on gas velocity. The ε_{trans} and u_{trans} mark the transition between the so-called homogeneous flow regime and the heterogeneous flow regime. Most correlations in literature[4-7] describe this transition point as a function of operating conditions, among which are pressure and column size.

However, this split-up of the gas-liquid slurry flow in only two

V. P. Chilekar is also affiliated with Reactor and Catalysis Engineering, Delft University of Technology, Julianlaan, The Netherlands
Correspondence concerning this article should be addressed to J. van der Schaaf at j.vanderschaaf@tue.nl.

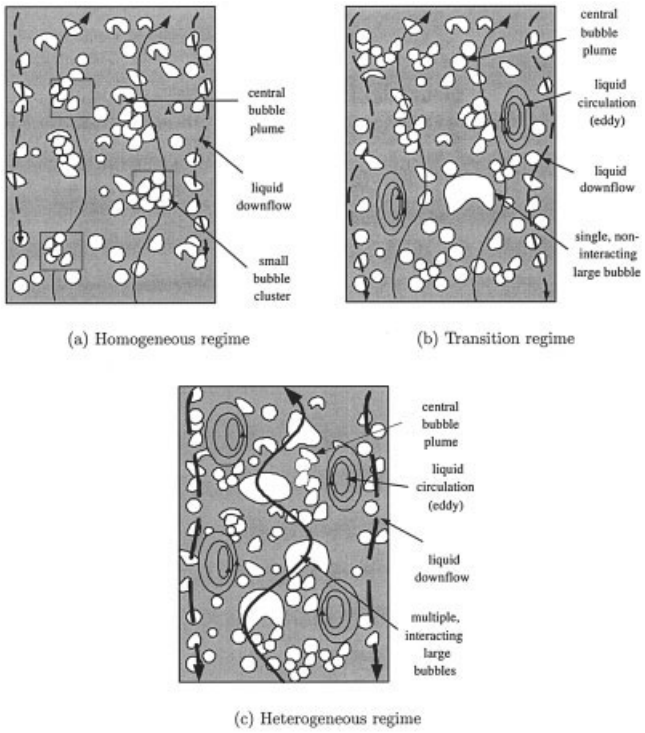

Figure 1. Three flow regimes in slurry bubble columns.

The corresponding images captured from high speed video recordings are shown in Figure 4. The wavelike motion of the fast bubble flow region in 2-D columns becomes a spiral flow motion in 3-D columns.

flow regimes and one transition point is actually an oversimplification. Presently, it is generally accepted that three flow regimes with two flow regime transition points can be identified, viz., the homogeneous regime, the transition regime, and the heterogeneous regime. Detailed descriptions of these regimes can be found in the literature.[8-13] By definition, the so-called first transition point separates the homogeneous regime and the transition regime, while the second transition point separates the transition regime and the heterogeneous regime. Figure 1 gives a view of the main flow phenomena that are associated with these three flow regimes. Obviously, a proper estimation of the gas holdup in these flow regimes depends strongly on an accurate prediction of the two transition points.

In literature, various experimental methods have been described to characterize flow regimes and transition points in slurry bubble columns using analyses of pressure fluctuation measurements, for example:

- statistical analysis,[14-16]
- fractal and chaos analysis, [15-21]
- time-frequency analysis using wavelet transform,[16,22]
- autocorrelation function,[14,21]
- average cycle frequency.[23]

Of course, other flow regime transition methods based on the measurement of the gas holdup are also well-known.[24-30] However, these methods suffer from a lack of accuracy due to the only very small differences between the slopes of the "ε_g vs. u_g" curve, when a transition happens. The slope changes gradually, and not abruptly, which most often obscures the identification of the transition point.

Despite the ubiquity of literature on the topic, the detection of the two transition points using pressure time series, in order to separate the three regimes, is still difficult. An important reason is that a universally accepted and unique experimental criterion to pinpoint the transition points in slurry bubble columns is still lacking. This is largely due to the fact that the analysis techniques mentioned previously, almost all rely on the arbitrary choice of specific parameters in the analysis method, and, therefore, give ambiguous transition points. As a result of this, no significant improved understanding is obtained. Also some of these methods are rather complicated, which hinders the interpretation of the results.[31]

In this article, we will demonstrate that the changes in the coherent standard deviation, and the average frequency of pressure-time series with gas velocity are simple and unique indications of the two flow regime transition points in slurry bubble columns. The coherent standard deviation clearly marks the first and the second regime transition points, while the average frequency can be used additionally to confirm the second transition point. The coherent standard deviation and the average frequency can be calculated from pressure time series using the discrete Fourier transform (DFT) technique. This technique is straightforward, and can be readily applied without the need of an arbitrary choice of analysis parameters. Moreover, the dependence of the coherent standard deviation and the average frequency on the gas velocity is closely related to the actual physical flow phenomena in the slurry bubble column that are underlying the pressure fluctuations. In particular, it will be demonstrated that the coherent standard deviation and the average frequency in the regime transition points are closely associated with the size and the frequency of occurrence of the large bubbles. At the first transition point, marking the transition from the homogeneous to the transition regime, the first large bubbles are detected. In the transition regime, from the first to the second transition point, the average diameter and the frequency of occurrence of the large bubbles increase with gas velocity. At the second transition point, marking the transition from the transition regime to the heterogenous regime, these quantities become constant.

We present pressure time series measurements in a 2-D slurry bubble column. The dependence of the coherent standard deviation and the average frequency of these pressure time series on the gas velocity will be shown. Simultaneously, the results of high-speed video imaging of the bubble flow behavior, viz., bubble diameter and frequency of occurrence of the large bubbles, will be clearly related to the pressure time series analyses. Finally, we will show that the coherent standard deviation and the average frequency can also be used to indicate the regime transitions in a 3-D slurry bubble column.

In the next two sections, we will first describe briefly which physical phenomena generate pressure fluctuations in a slurry bubble column, and then give a short description of the calculation of the coherent standard deviation and the average frequency of pressure time series.

Physical phenomena underlying pressure fluctuations

Pressure fluctuations in slurry bubble columns can be divided in global and local pressure fluctuations:

- Global pressure fluctuations are caused by bubble coalescence, bubble breakup, bubble eruption, bubble formation,

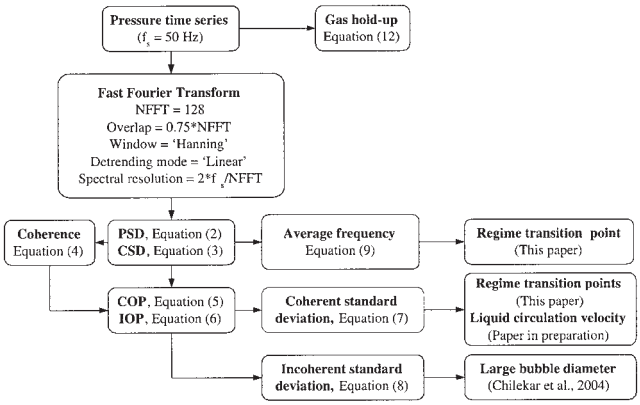

Figure 2. Algorithm of detecting regime transitions, liquid circulation velocity, and large bubble diameter in slurry bubble columns using pressure time series.

The calculation file is written in Matlab® software 6.0 and can be downloaded from our Web site (www.chem.tue.nl/scr).

natural oscillations of the slurry suspension,[32] and column mechanical vibrations.[33] Global pressure fluctuations generate pressure waves traveling upward and downward from their origin. These pressure waves are measured almost instantaneously throughout the entire column because of their high propagation velocity (> 50 m s^{-1}).[34] Therefore, these global pressure waves are coherent and have a constant time shift of nearly zero, when measured simultaneously at two different heights in the column.

- Local pressure fluctuations are caused by liquid velocity fluctuations, due to rising gas bubbles, large eddies, turbulence, and gas holdup fluctuations, due to the passage of large gas bubbles. Abrupt changes in the liquid velocity occur when liquid is dragged upward by large bubbles or when large eddies move up or down in the column. These pressure fluctuations travel with the velocity of the source itself (< 2 m s^{-1}), and are only measured in the vicinity of the source. For example, gas bubbles are formed at the distributor plate and change size, shape, and velocity as they rise in the column. These changes are not detected below or above the gas bubble. Consequently, at higher measurement positions, the pressure fluctuations due to passing gas bubbles are incoherent with the pressure fluctuations measured at the distributor plate, where large bubbles are not yet present.

Thus, the coherence between a pressure time series measured at the distributor plate and one measured at any other location in the column can be used to separate phenomena related to fast-traveling pressure waves (with high coherence) from those resulting from slow-traveling waves (with low coherence), such as rising large gas bubbles. This enables the estimation of the large bubble size from pressure fluctuation measurements,[35;36] while also information can be obtained to characterize flow regimes and to detect flow regime transitions, as we will demonstrate in this article (see Figure 2).

Spectral analysis of pressure time series

In this article, discrete Fourier transform (DFT) is used to calculate the coherent standard deviation and the average frequency from pressure time series measured at the wall of 2-D and 3-D slurry bubble columns. DFT converts the pressure time series from the time domain to the frequency domain.[37] The discrete Fourier transform $\mathcal{F}_x$, of a pressure time series measured at position x, P_x, is defined as

$$\mathcal{F}_x(f) = \frac{1}{N}\sum_{n=0}^{N-1} P_x(t_n)e^{-j2\pi ft_n/N} \tag{1}$$

The power spectral density (PSD) of a pressure time series measured at position x, Φ_{xx}, is defined as

$$\Phi_{xx}(f) = \frac{1}{f_s}\mathcal{F}_x(f)\mathcal{F}_x^*(f) \tag{2}$$

where $\mathcal{F}_x^*$ is the complex conjugate of F_x, and f_s is the sample frequency. The cross power spectral density (CSD) is calculated from two pressure time series measured at positions x and y as

$$\Phi_{xy}(f) = \frac{1}{f_s}\mathcal{F}_x(f)\mathcal{F}_y^*(f) \tag{3}$$

The value of the cross power spectral density will be high for a given frequency if the Fourier transforms of both time series at that frequency have a constant phase shift: the time series are coherent for that frequency. The cross power spectral density depends on the power present in the PSDs of both pressure time series. The coherence can be used to eliminate this dependence.[37] For this purpose, the absolute value of the cross power spectral density is normalized with the square root of the PSDs of both pressure time series. The square of this value is known as the coherence, γ_{xy}^2, which ranges from 0 to 1

$$\gamma_{xy}^2(f) = \frac{\Phi_{xy}(f)\Phi_{xy}^*(f)}{\Phi_{xx}(f)\Phi_{yy}(f)} \tag{4}$$

The coherence can be used to separate local pressure fluctuations from global pressure fluctuations. Just above the gas distributor plate, no large gas bubbles are present; they are formed at higher positions in the column. Thus, at the gas distributor, predominantly global pressure fluctuations are measured. Now, the coherence can be used to indicate whether the phenomena generating global pressure waves are dominant, corresponding to a high coherence, or whether the phenomena generating local pressure waves are dominant, corresponding to a low coherence.[37] A coherence of unity at frequency f indicates that the PSDs of the pressure time series have a constant phase lag at that frequency. The power in the PSDs at that frequency may be different. A coherence between zero and unity at frequency f indicates the amount of power in the PSDs of the pressure time series that has a constant phase lag. The coherence is zero for completely uncorrelated pressure time series.

The power in both time series can be expressed in terms of the coherent-output power spectral density (COP), and the incoherent-output power spectral density (IOP), representing the PSDs due to

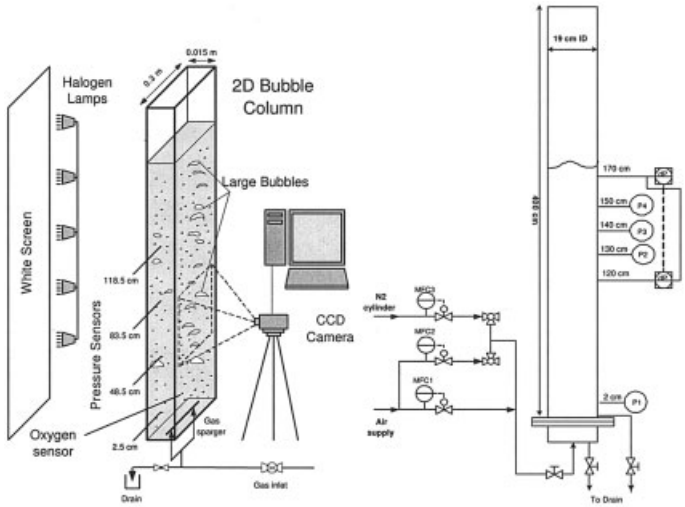

Figure 3. (a) 2-D perspex bubble column, dimension of thickness ×width ×height of 0.015 × 0.30 × 2.00 m^3, with Druck pressure sensor connections located at a height of 0.025 m, 0.485 m, 0.835 m, and 1.185 m above the gas sparger for pressure time series measurements, and (b) shows a 3-D perspex bubble column, dimension of dia. × height of 0.19 × 4m^2, with Validyne pressure sensor connections located at a height of 1.2 m and 1.7 m, and Kistler pressure sensor connections located at a height of 0.02 m, 1.3 m, 1.4 m, and 1.5 m above the gas sparger.

A perforated plate sparger with a triangular pitch of 7 mm with 0.5 mm dia. holes was used for both set-ups. The gas flow was controlled by mass flow controllers.

global (correlated) pressure fluctuations, and due to local (uncorrelated) pressure fluctuations, respectively[35,36]

$$\mathrm{COP}_y(f) = \gamma_{xy}^2(f)\Phi_{yy}(f) \tag{5}$$

$$\mathrm{IOP}_y(f) = (1 - \gamma_{xy}^2(f))\Phi_{yy}(f) \tag{6}$$

Equation 6 shows that the IOP at position y represents the power of the local pressure fluctuations present in the pressure time series measured at position y. From the coherent output and incoherent-output PSDs, the coherent standard deviation σ_c, and the incoherent standard deviation, σ_i, can be calculated, according to Parseval's theorem[38] (that is, the area under a PSD-curve is equal to the variance of the corresponding pressure time series, σ^2)

$$\sigma_i^2 = \int_0^\infty \mathrm{IOP}(f)\mathrm{d}f \tag{7}$$

$$\sigma_c^2 = \int_0^\infty \mathrm{COP}(f)\mathrm{d}f \tag{8}$$

The average frequency $\bar{f}_y$ of the pressure fluctuations at position y can be determined from the PSD as

$$\bar{f}_y = \frac{\Sigma_i f_i \Phi_{yy}(f_i)}{\Sigma_i \Phi_{yy}(f_i)} \tag{9}$$

where $\Phi(f_i)$ is the power at frequency f_i obtained from the PSD. The average frequencies of the coherent part and the incoherent part of the pressure time series are defined as

$$\bar{f}_{\mathrm{COP}} = \frac{\Sigma_i f_i \mathrm{COP}_y(f_i)}{\Sigma_i \mathrm{COP}_y(f_i)} \tag{10}$$

$$\bar{f}_{\mathrm{IOP}} = \frac{\Sigma_i f_i \mathrm{IOP}_y(f_i)}{\Sigma_i \mathrm{IOP}_y(f_i)} \tag{11}$$

In this article, we will demonstrate that the coherent standard deviation σ_c^2, and these average frequencies can effectively be used to characterize flow regimes and detect flow regime transitions. The two methods for detecting regime transitions are illustrated in Figure 2.

Experimental setup and procedure

The 2-D slurry bubble column is shown in Figure 3a. All experiments were carried out with demineralized water and nitrogen gas at ambient pressure and temperature. A perforated plate sparger was used with a triangular pitch of 7 mm with 0.5 mm dia. holes. Total number of holes in the sparger is 49. The dimensions of the sparger are 200 × 15 × 5 mm^3 (height × width × thickness). The gas flow was controlled by mass-flow controllers.

The 3-D slurry bubble column is shown in Figure 3b. All experiments were carried out with demineralized water and air at ambient conditions. A perforated plate sparger was used with a triangular pitch of 7 mm with 0.5 mm dia. holes. Total

Table 1. Physical Properties of the Catalyst Support Particles Used in the 2-D and 3-D Slurry Bubble Column

Support	Silica	Carbon	Support	Silica	Carbon
Code	G-5268	43242	Pore width [nm]	8.6	9.2
d_p [μm][1]	44	30	$V_{s,p}$ [ml g^{-1}][4]	1.63	1.60
ρ_s [kg m^{-3}][2]	2130	1300	ε_p [$-$][4]	0.70	0.65
S_{BET} [m^2 g^{-1}][3]	485	850	ΔH_i [mJ m^{-2}][5]	-201	-54

1. Measured using Coulter counter LS 130 in an aqueous suspension. Carbon particle size distribution 5% $<$ 2.5 μm, 50% $<$ 24 μm, 90% $<$ 100 μm. Silica particle size distribution 10% $<$ 18 μm, 50% $<$ 43 μm, 90% $<$ 95 μm.
2. Solid particle density measured using Micromeritics multivolume pycnometer.
3. Specific surface area measured using N_2 physisorption in Micromeritics ASAP-equipment.
4. Pore volume measured using mercury porosimetry in Micromeritics Autopore IV 9500, where porosity is calculated using $\varepsilon_p = (V_{s,p}\rho_s)/(1 + V_{s,p}\rho_s)$ and verified using $\rho_s = \rho_{p_g}/(1 - \varepsilon_p)$.
5. Heat of immersion in demineralized water from a Calvet C-80 microcalorimetry.

number of holes in the sparger is 550. The dimensions of the sparger are 170 $\times$ 5 mm^2 (dia. $\times$ thickness). The gas flow was controlled by mass flow controllers.

Two different particle types were used: silica and carbon particles. The physical properties are given in Table 1. The particles were prewashed with demineralized water to remove possible contamination. The particles were stored at 363 K to keep them dry. To ensure that all particles were completely wetted before each measurement, the particles were mixed with demineralized water for 45 min outside the column and a stabilization time of 10 min was allowed inside the column, before each experimental reading. The same batches of carbon and silica particles were used in the 2-D and 3-D columns.

Pressure time series

In the 2-D column, pressure time series were recorded simultaneously with four fast dynamic pressure sensors (Druck PTX 1400) which measure the pressure with respect to atmospheric pressure. They were mounted on the back plate of the 2-D column as shown in Figure 3a. The local pressure signal was recorded for 120 s with a sample frequency of 50 Hz. The combined nonlinearity, hysteresis, and repeatability accuracy of the Druck sensor is 0.25% of the full scale output (40 kPa).

In the 3-D column, pressure time series were recorded with two dynamic pressure sensors (Validyne DP 15) connected at heights of 1.2 and 1.7 m above the distributor, and with four dynamic pressure sensors with high pass filter (Kistler type 7261) connected at heights of 0.02 m, 1.3 m, 1.4 m, and 1.5 m, as shown in Figure 3b. The pressure time signals were recorded for 120 s with a sample frequency of 100 Hz and filtered at 50 Hz using a Scadas II data acquisition system (LMS, Breda, The Netherlands). The combined nonlinearity, hysteresis, and repeatability accuracy of the Validyne sensor is 0.25% of the full scale output (5.5 kPa). The combined nonlinearity, hysteresis, and repeatability accuracy of the Kistler sensor is 0.8% of the full scale output (set to 2 kPa). The Kistler pressure transducer measures the pressure fluctuations relative to the average pressure with a repeatability error less than 2 Pa.

The power spectral density of the fluctuating part of the pressure signal was estimated from a time series of 6,000 points (using Matlab® 6.0), divided in segments of 128 points each, using an overlap of 75% of this block length and a Hanning window to prevent edge effects. The spectral resolution is 0.39 Hz over a frequency range of 0 to 25 Hz. Each block was linearly detrended to prevent offset accumulation below the spectral resolution.

Gas holdup

The pressure difference between two pressure sensors was used to estimate the local gas hold-up according to Eq. 12

$$\varepsilon_{i,j}^{local} = \frac{(\bar{p}_j - \bar{p}_i)_0 - (\bar{p}_j - \bar{p}_i)_{aerated}}{(\bar{p}_j - \bar{p}_i)_0} \quad \text{where } i, j = 1\text{–}4, j > i \tag{12}$$

where i and j represent the pressure sensor positions on the column wall, and $\varepsilon_{3,4}$ represents the total gas holdup. The initial liquid height in the 2-D column was between 1.2 and 1.4 m ensuring that the gas holdup was independent of liquid height (only above 1 m) in agreement with Kluytmans et al..[23] The initial liquid height in the 3-D column was between 1.7 and 1.8 m to ensure that the gas holdup was independent of liquid height (only above 0.8 m).[12]

Table 2. Transition Gas Velocity and Corresponding Transition Gas Holdup at the First Transition Point Based on the Coherent Standard Deviation of Pressure Time Series for Demineralized Water, Silica, and Carbon Particle Slurries in the 2-D and 3-D Slurry Bubble Columns (1 bar, 295 K)

2-D Column ($-$)	u_{trans} (m s^{-1})	ε_{trans} ($-$)	3-D Column ($-$)	u_{trans} (m s^{-1})	ε_{trans} ($-$)
Demi. water	0.060	0.170	Demi. water	0.090	0.280
0.5 g l^{-1} carbon	0.063	0.168	0.5 g l^{-1} carbon	0.090	0.270
1 g l^{-1} carbon	0.060	0.170	1 g l^{-1} carbon	0.085	0.250
2 g l^{-1} carbon	0.055	0.174	2 g l^{-1} carbon	0.080	0.240
4 g l^{-1} carbon	0.055	0.177	5 g l^{-1} carbon	0.070	0.208
0.5 g l^{-1} silica	0.060	0.189	0.5 g l^{-1} silica	0.090	0.260
1 g l^{-1} silica	0.063	0.187	1 g l^{-1} silica	0.085	0.261
2 g l^{-1} silica	0.063	0.193	2 g l^{-1} silica	0.080	0.250
5 g l^{-1} silica	0.060	0.187	5 g l^{-1} silica	0.070	0.212

High speed video imaging

A high shutter speed Dalsa CA-D6 video camera (Tech5, The Netherlands) was used to record video images at a frame rate of 955 Hz, at a height of 58 cm above the sparger in the 2-D bubble column. The frame size was 0.3 m × 0.3 m with a resolution of 256 × 256 pixels. It was used to determine the average large bubble size, the frequency of occurrence of large bubbles, and the bubble rise velocities in the 2-D bubble column. The recorded video images were processed and analyzed with image processing software developed at our laboratory,[39] based on Matlab® software. Since the distance between the perspex plates of the 2-D column was 15 mm, only bubbles with a diameter larger than 15 mm touched both the walls of the column. The large bubble population was assumed to start from bubbles with a bubble area of 100 pixels (equivalent to a bubble dia. of 13.7 mm). The objects smaller than 100 pixels were considered to be small bubbles. The volume of the small bubbles was calculated by subtracting the volume of the large bubbles (obtained from image analysis) from the total gas volume (obtained from pressure measurements using Eq. 12). On the basis of the bubble size classification of Krishna et al.[40] and visual study of the video images, bubbles smaller than the depth of the column (15 mm) were assumed equal in size with a dia. of 8 mm. The area-averaged large bubble dia., $<d_{b,large}>$, was calculated from

$$d_{b,large,i} = \sqrt{\frac{4}{\pi}\left(\frac{\sum_{j=1}^{n} \text{Area}_{j,i}}{n}\right)} \tag{13}$$

$$w_i = \frac{\Delta d_{x,i}}{0.3 - d_{b,large,i}} \tag{14}$$

$$N_{bubbles} = \sum_{i=1}^{m} (w_i) \tag{15}$$

$$\langle d_{b,large} \rangle = \sqrt{\frac{\sum_{i=1}^{m} (d_{b,large,i})^2 w_i}{N_{bubbles}}} \tag{16}$$

where i is the index of objects considered as bubble, j is the frame number, n is the number of frames in which bubble i is detected, Δd_x is the total distance in height traveled by a large bubble in the captured area, w is the weighting factor (equal to Δd_x divided by the maximum distance it could have traveled), m is the total number of objects considered as bubble, $N_{bubbles}$ is the total number of bubbles, and Area $_{j,i}$ is the area of all the objects i in frame number j.

The frequency of occurrence of large bubbles, that is, number of large bubbles passing through the column per s, was calculated as

$$F_{b,large} = \frac{N_{bubbles}}{\Delta t} \tag{17}$$

where Δt is the length of the movie in real time. One movie of 10,000 frames corresponds to 10.5 s for one gas velocity.

The small gas bubble holdup was calculated from the total gas holdup as determined from the pressure difference (Eq. 12) minus the large gas bubble holdup as determined from the image analysis. A total of 58 movies were recorded for a silica particle slurry in the concentration range of 0.25 to 5.0 g l^{-1}, and a total of 60 movies were recorded for a carbon particle slurry in the concentration range of 0.1 to 1.0 g l^{-1}. Further details of the image analysis software, and the video movies are available on our website: http://www.chem.tue.nl/scr.

Experimental Results

2-D slurry bubble column

Figure 4 shows typical pressure fluctuations around the average pressure (sensor P3, 2-D column), and the corresponding video snapshots at five different gas velocities for the silica particle slurry, corresponding to the three low regimes and the two transition points. For each gas velocity, the image is a representative frame out of 10,000 frames. The following observations are made:

- In the homogeneous regime (Figure 4 A), the diameter of the gas bubbles is approximately 3 to 10 mm. Only these small gas bubbles generate pressure fluctuations as they rise upward in the column. The variance of the pressure signal is small (σ = 36 Pa at u_g = 0.045 m s^{-1}). In the video, liquid phase circulations and clusters of small bubbles are already observed. The liquid moves upward in the center of the column and downward at the wall.
- At the first transition point (Figure 4 A → B), the first large bubbles of approximately 15 mm are detected with a low frequency of occurrence. The amplitude of the pressure signal is still small (σ = 136 Pa).
- In the transition regime (Figure 4 B), the diameter and the frequency of occurrence of the large gas bubbles increase strongly with increasing gas velocity. The amplitude of the pressure signal increases (σ = 413 Pa at u_g = 0.103 m s^{-1}). The liquid phase circulations are more intense.
- At the second transition point (Figure 4 B → C), the large bubble size reaches an equilibrium diameter of approximately 50 mm, and the frequency of occurrence also levels off. The amplitude of the pressure signal increases (σ = 565 Pa).
- In the heterogeneous regime (Figure 4C), the amplitude of the pressure fluctuations increases to high values (σ = 980 Pa at u_g = 0.224 m s^{-1}). These high values are caused by very large liquid circulations and large gas bubbles.

The PSDs of pressure time series for demineralized water and carbon particle slurry systems are shown in Figures 5a and 5c. The dotted lines in the figure represent the power at intermediate gas velocities. In the homogeneous regime, the power in the PSD increases uniformly over a complete frequency range as a function of gas velocity. Only the power in the PSD at frequencies lower than 2 Hz exceeds the noise level of approximately 10 Pa^2/Hz. A broad peak is present around 10 Hz, where the power increases from 10 to 100 Pa^2/Hz with a gas velocity increase from 0.01 to 0.07 m s^{-1}. For the same gas velocity increase, the power around 0.5 Hz (the spectral resolution is 0.39 Hz) increases from 2 to 500 Pa^2/Hz. This power is present in the pressure signals at all sensor locations. This may correspond to noise and/or liquid circulations and holdup fluctuations at the low frequency range of 0 to 1 Hz[14]. The power is lower at position P1 than at the other locations, especially for higher gas velocities. In the transition regime, the

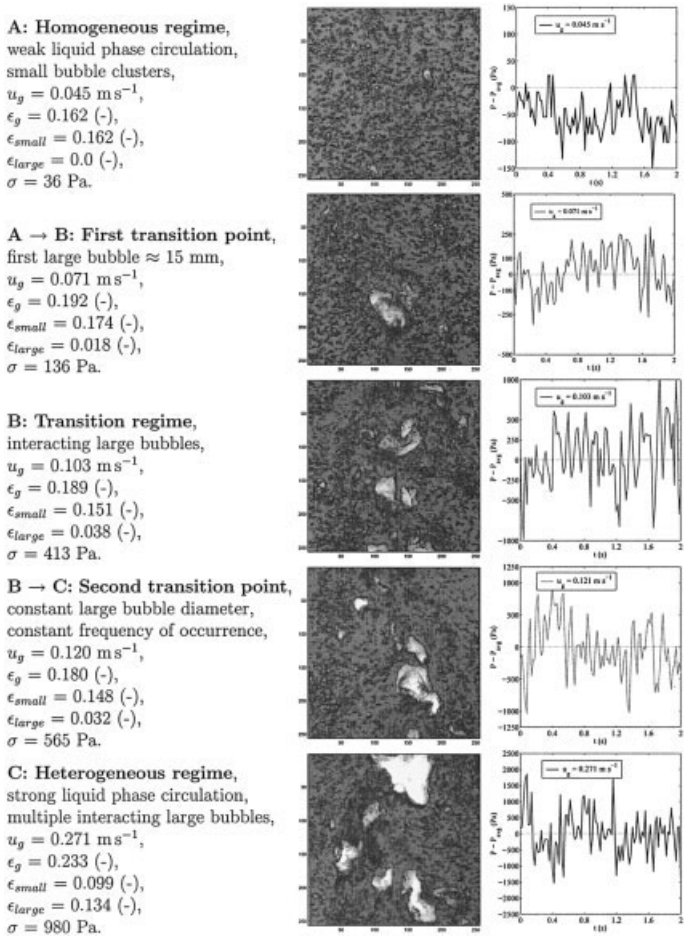

Figure 4. Images captured between 58 and 88 cm above the sparger between the positions of pressure sensors P2 and P3 and typical pressure fluctuations around the average pressure from the pressure sensor P3 for a 2 g l^{-1} silica slurry in a 2-D slurry bubble column.

Image size is 30 × 30 cm^2.

power increases rapidly first at the lower frequencies (<4 Hz), followed by an increase at the higher frequencies (7 to 12 Hz). In the heterogeneous regime, a constant distribution of power over all frequencies is observed. The average frequency calculated from the PSD is shown in Figure 6 for demineralized water and carbon particle slurry. The average frequency first decreases with increasing gas velocity, attains a minimum at $u_g = 0.07$ m s^{-1}, and then increases up to a constant value of 8 Hz till $u_g = 0.12$ m s^{-1}, with increasing gas velocity (see also Figure 11).

The coherence between the pressure time series measured with sensor P1 and sensor P3 is calculated for all gas velocities using Eq. 4. For very low gas velocities, $u_g < 0.03$ m s^{-1}, there is a moderate coherence, up to 0.25 (-), for a frequency range of 5 to 15 Hz, and up to 0.4 (-) for a frequency range of 20 to 25 Hz for sensor P3 w.r.t. sensor P1. This coherence is possibly due to small fluctuations in the liquid circulation velocity or by small gas bubble formation. Once the gas velocity is increased and more bubbles are present, the coherence of the measured pressure fluctuations at these frequencies has a negligible influence on the PSD. For $u_g > 0.07$ m s^{-1}, there is a high coherence up to 0.6 (-) at a frequency range of 2 to 4 Hz. From the coherence and the PSD, the IOPs and COPs are calculated for sensor P3 for each gas velocity (Figures 7a and 7b). The coherent and incoherent standard deviations, and the average frequency against gas velocity are affected by the amplitude of the power in the PSD, IOP and COP, results of which are shown in Figure 8.

The average large bubble diameter and the frequency of occurrence of the large bubbles are calculated from the video recordings (Figure 9). The gas holdup versus gas velocity as a function of silica particle concentration is shown in Figure 14a. Similar results are also obtained for carbon particle slurries. The gas holdup decreases with increasing particle concentration, which is attributed to the coalescence promotion by the added particles.

3-D slurry bubble column

For the 3-D slurry bubble column, the PSDs of pressure time series for demineralized water and carbon particle slurry are shown in Figures 10a and 10b. The dotted lines in the figure represent the power at the intermediate gas velocities. A more accurate Kistler pressure sensor was used with a noise level of approximately 0.1 Pa^2/Hz. A broad peak is present around 10 Hz, where the power increases from 7 to 100 Pa^2/Hz with a gas velocity increase from 0.01 to 0.08 m s^{-1}. For the same gas velocity increase, the power around 0.5 Hz increases from 2 to 1,000 Pa^2/Hz. In the transition regime, the power increases

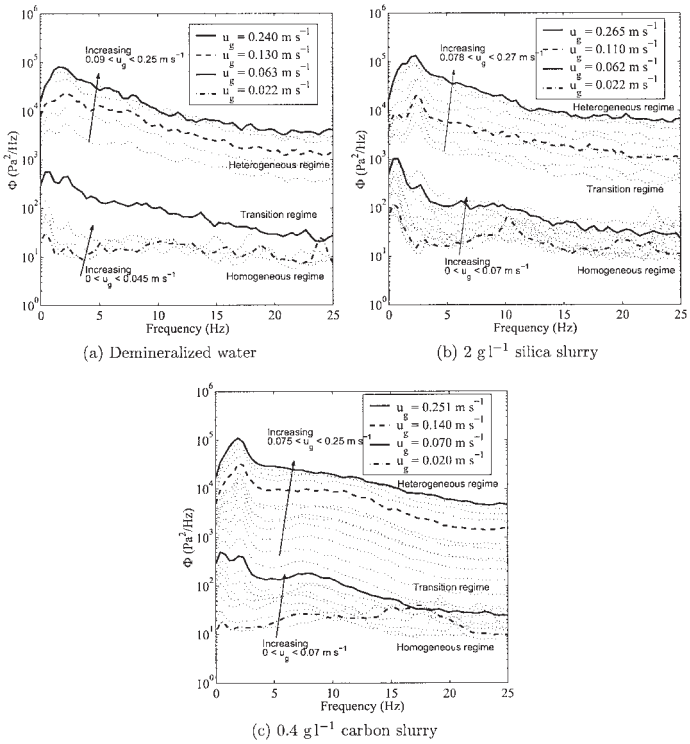

Figure 5. Semilog plot of the power spectral density against frequency as a function of superficial gas velocity in a 2-D (slurry) bubble column.

rapidly first at the lower frequencies (below 4 Hz) followed by an increase at the higher frequencies (7 to 12 Hz). In the heterogeneous regime, a constant distribution of power over all frequencies is observed. The average frequency calculated from the PSD is shown in Figures 11a and 11b for demineralized water and carbon particle slurry. The average frequency first decreases with increasing gas velocity, attains a minimum at $u_g = 0.10$ m s^{-1}, stays at the same minimum for a while, and then increases from $u_g = 0.17$ m s^{-1} up to a constant value of 5 Hz, with increasing gas velocity. Where the average frequency starts increasing from its minimum, the gas holdup attains a local maximum. Where the average frequency becomes constant and does not increase further with gas velocity, the gas holdup attains a local minimum. From the coherence and the PSD, the IOPs and COPs are calculated for the pressure time series measured with sensor P3 for each gas velocity (Figures 12a and 12b). The coherent and the incoherent standard deviations of pressure fluctuations are shown in Figures 13a and 13b, respectively. The gas hold-up versus gas velocity as a function of silica particle concentration is shown in Figure 14b. Similar results are also obtained for carbon particle slurries. The gas holdup decreases with increasing particle concentration, which is attributed to the coalescence promotion by the added particles.

Flow Regimes and Transition Points

In this section, it is demonstrated how the coherent standard deviation and the average frequency of pressure time series can be used to uniquely pinpoint the transitions between the homogeneous and the transition regimes (first transition point), and between the transition and the heterogeneous regimes (second transition point). In this way, clear criteria are obtained to determine these transition points in 2-D and 3-D slurry bubble columns. First, the 2-D slurry bubble column data will be discussed, followed by the 3-D slurry bubble column results.

2-D slurry bubble column

Homogeneous regime. In the homogeneous regime, from video recordings in the 2-D column, it is found that at $u_g < 0.02$ m s^{-1}, the small bubbles (3 – 8 mm dia.) in the column are uniformly distributed. With increasing gas velocity, the small bubbles start to form clusters (Figure 4a). These small bubble clusters have also been reported earlier,[10,41] and are formed as a result of local liquid circulation patterns.[13] At $u_g = 0.06$ m s^{-1}, the small bubble clusters consist of approximately 20 – 30 small bubbles, some of which coalesce to form single noninteracting large bubbles (approximately 15 mm dia.), see also Figure 9. In this regime, the small bubbles generate power in the PSD specifically at higher frequencies in the range of 10 – 25 Hz (Figures 5a and 5c). Therefore, initially a high average frequency is observed (Figure 6). The average frequency decreases with gas velocity because of more power at the lower frequencies due to the ever growing formation of small bubble clusters. Figure 8a shows the coherent standard deviation and Figure 8b shows the incoherent standard deviation for pressure sensors P2, P3, and P4 as a function of superficial gas velocity. For $u_g < 0.06$ m s^{-1}, σ_c is constantly nearly zero, while σ_i is only slightly greater than zero and increases with gas velocity.

First transition point

In the homogeneous regime, the point where σ_c starts increasing ($u_g = 0.06$ m s^{-1}) corresponds to the appearance of

the first large bubbles with a diameter of 1.5 cm. The sigmoidal curve of the average large bubble diameter against gas velocity has a sharp increase at this point (Figure 9). Therefore, this point is regarded as the first transition point which marks the onset of the transition regime. At this first transition point, the frequency of occurrence of the large bubbles is small (around one bubble per s). Therefore, the contribution of the large bubbles to the power in the PSD is small and, hence, the average frequency keeps on decreasing with gas velocity.

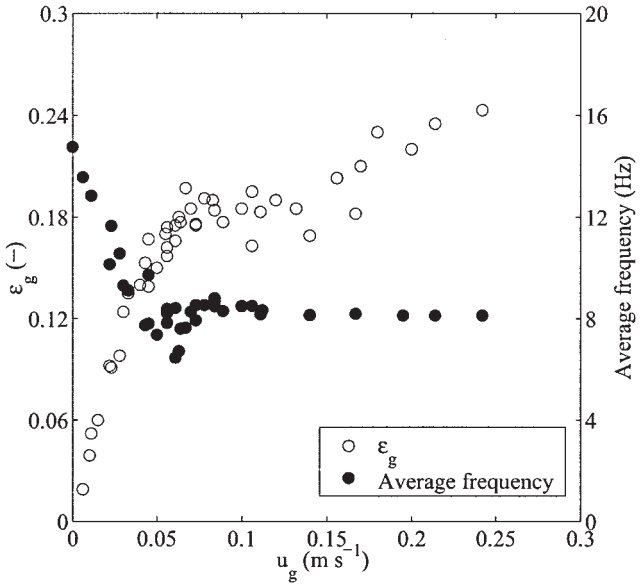

(a) Demineralized water

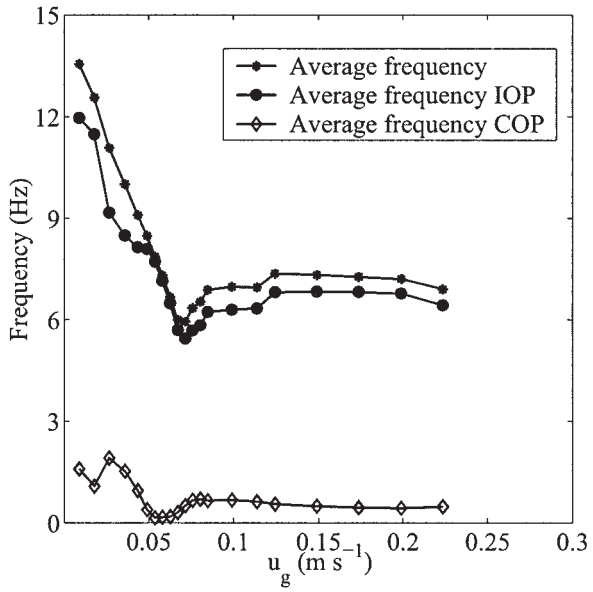

(b) 0.5 g l^{-1} carbon slurry

Figure 6. Gas holdup and average frequency of measured pressure time series against superficial gas velocity measured in a 2-D slurry bubble column for carbon and silica particle slurries.

The average frequency of IOP and COP against gas velocity is also shown for sensor P3.

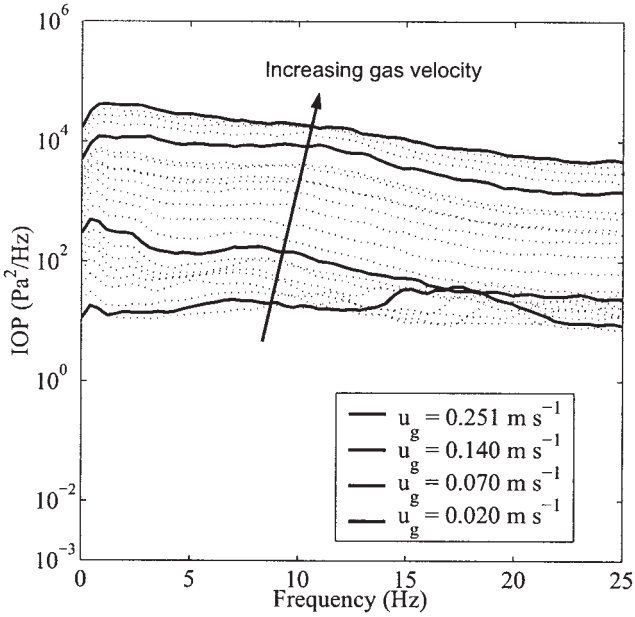

(a) IOP

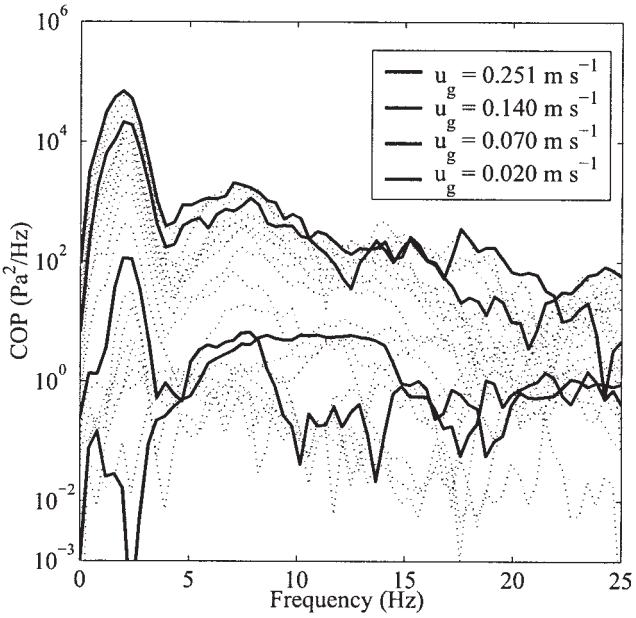

(b) COP

Figure 7. Semilog plot of the incoherent output power (IOP) and the coherent output power (COP) against frequency as a function of superficial gas velocity for 0.5 g l^{-1} carbon particle slurry in a 2-D slurry bubble column.

Transition regime

In the transition regime, the amplitude of the pressure fluctuations increases with increasing gas velocity (Figure 4), bubble coalescence and large bubble breakup start, the rise velocity of the large bubbles increases, and the gas holdup decreases. The formation of large bubbles gradually overshadows the small bubbles pressure fluctuations. This is reflected in the

change in the shape and the power in the PSD, as shown in Figures 5a to 5c. For demineralized water, the power in the PSD between $u_g = 0.06$ and 0.10 m s^{-1} is significantly different from the power at the lower and higher gas velocities. For slurries of carbon and silica particles, the power in the PSD between 0.07 and 0.12 m s^{-1} is significantly different. The power and amplitude in the PSD in the frequency range of 2 to 4 Hz increase steadily with constant shape as the frequency of occurrence of large bubbles increases (Figure 9). For the silica and the carbon particle slurries (concentration less than 2 g l^{-1}), the average frequency does not

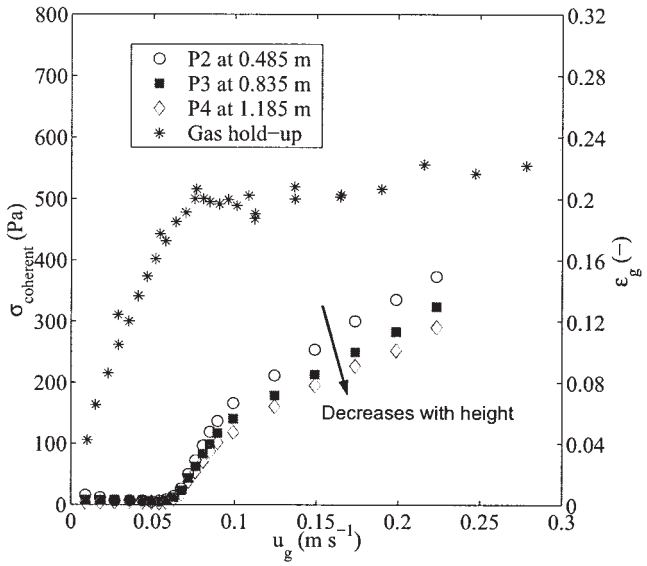

(a) Coherent standard deviation

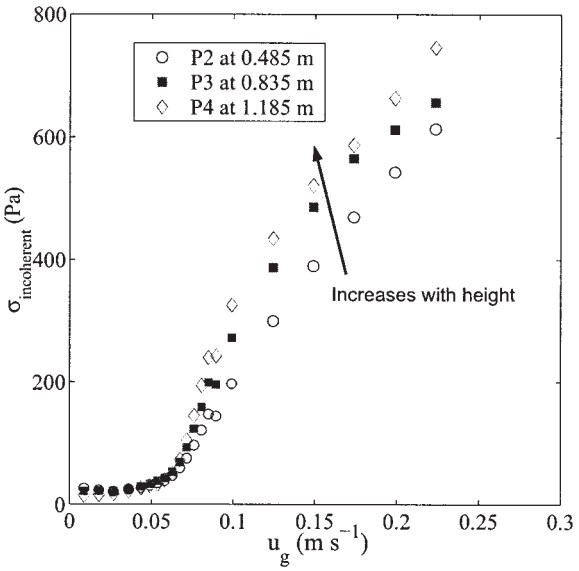

(b) Incoherent standard deviation

Figure 8. The standard deviation of the incoherent output power (IOP) and coherent output power (COP) against superficial gas velocity for 0.5 g l^{-1} carbon particle slurry in a 2-D slurry bubble column.

At $u_g = 0.06$ m s^{-1}, the coherent standard deviation starts increasing, which is referred to as the first transition point.

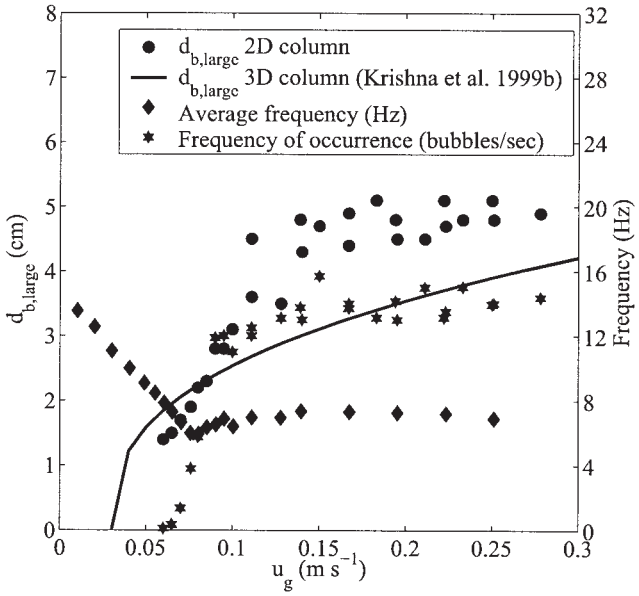

Figure 9. Average large bubble diameter and frequency of occurrence of large bubbles calculated from the image analysis.

The average frequency from the PSD of measured pressure time series is also given to compare its behavior with the frequency of occurrence of large bubbles. The data is calculated from 26 movies for 0.3–0.5 g l^{-1} carbon particle slurry. The solid line represents the large bubble diameter correlation developed for 3D bubble columns.

decrease further and attains a minimum at approximately $u_g = 0.07$ m s^{-1} (Figure 6). This minimum of the average frequency corresponds to the appearance of large bubbles of 2 to 3 cm dia. with a frequency of occurrence of approximately 6 bubbles per s (Figure 9). It is observed that the gas holdup against gas velocity curve does not always attain a local maximum at the gas velocity where the average frequency attains a minimum (Figure 6). At this minimum, the average frequency is in the range of 6 to 8 Hz (Figure 6). At the minimum point in the average frequency, the power in the PSD increases rapidly with more power at the higher frequencies (6 to 10 Hz) than at the lower frequencies (2 to 3 Hz) due to liquid velocity fluctuations created by large bubbles (see incoherent part of average frequency in Figure 6b). Hence, the average frequency increases with increasing gas velocity in the transition regime.

Figures 8a and 8b show that the coherent and the incoherent standard deviations both increase rapidly with increasing gas velocity. The coherent standard deviation of the pressure fluctuations of sensors P3 and P4 is lower than the coherent standard deviation at sensor P2 w.r.t. sensor P1 in the distributor region. Apparently, the coherent pressure waves are generated below pressure sensor P2 and are attenuated along with the column height. The incoherent standard deviation of the pressure fluctuations of sensors P3 and P4 is higher than the incoherent standard deviation at pressure sensor P2. Possibly, the number of large bubbles passing at sensor position P3 is higher than at sensor position P2.

Second transition point

In the transition regime, predominantly large bubbles (dia. 2 – 5cm) are present, however, their maximum size is still not

reached as is shown in Figure 9. The frequency of occurrence of these large bubbles is 10 to 15 bubbles per s. At $u_g = 0.12$ m s^{-1}, the average large bubble diameter and the frequency of occurrence of large bubbles become constant. This point is designated as the second transition point. The average diameter and the frequency of occurrence of large bubbles increase to 5 cm and 13 bubbles per s, respectively, and become constant after this second transition point. This second transition point is marked by the average frequency and the coherent standard deviation of pressure time series. At this transition point, the average frequency becomes independent of gas velocity, and the slope of the coherent standard deviation with gas velocity clearly decreases. Also, the gas holdup shows a local minimum. However, this is not generally observed for all the particle concentrations in this study (Figure 6). The observed increase in gas hold-up with gas velocity is due to an increase in the number of small gas bubbles. The second transition point marks the end of the transition regime and the start of the fully developed heterogeneous regime.

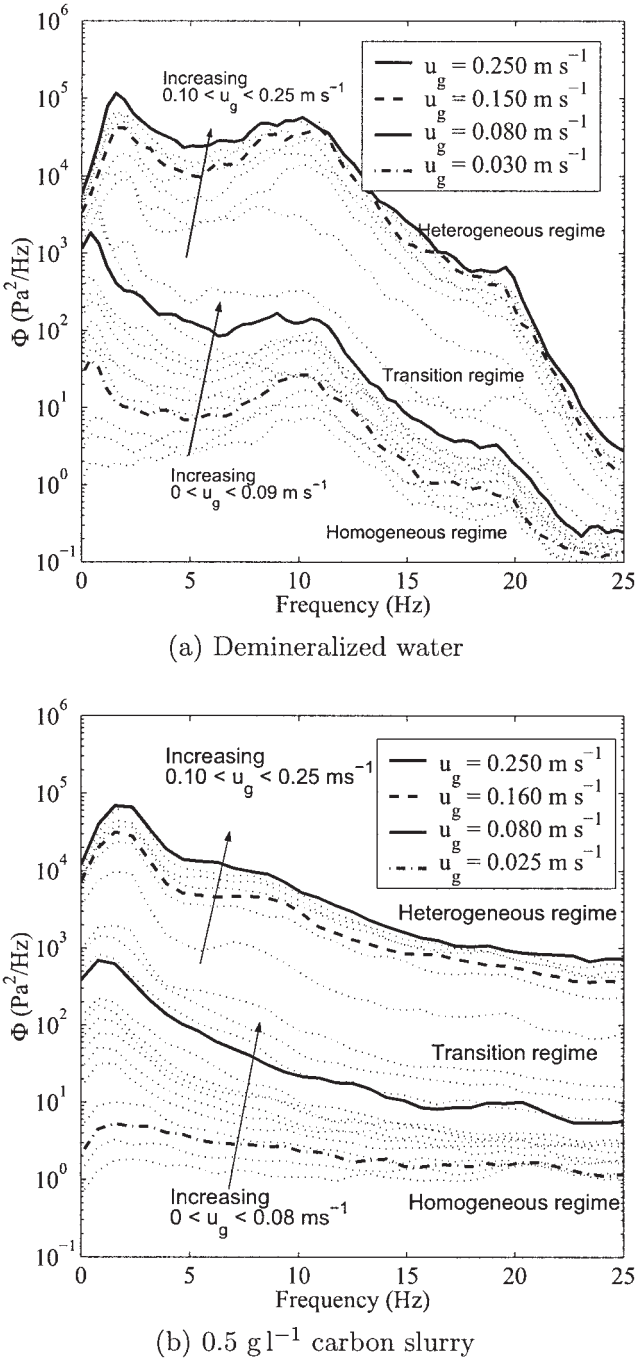

Figure 10. Semilog plot of the power spectral density against frequency as a function of superficial gas velocity in a 3-D (slurry) bubble column.

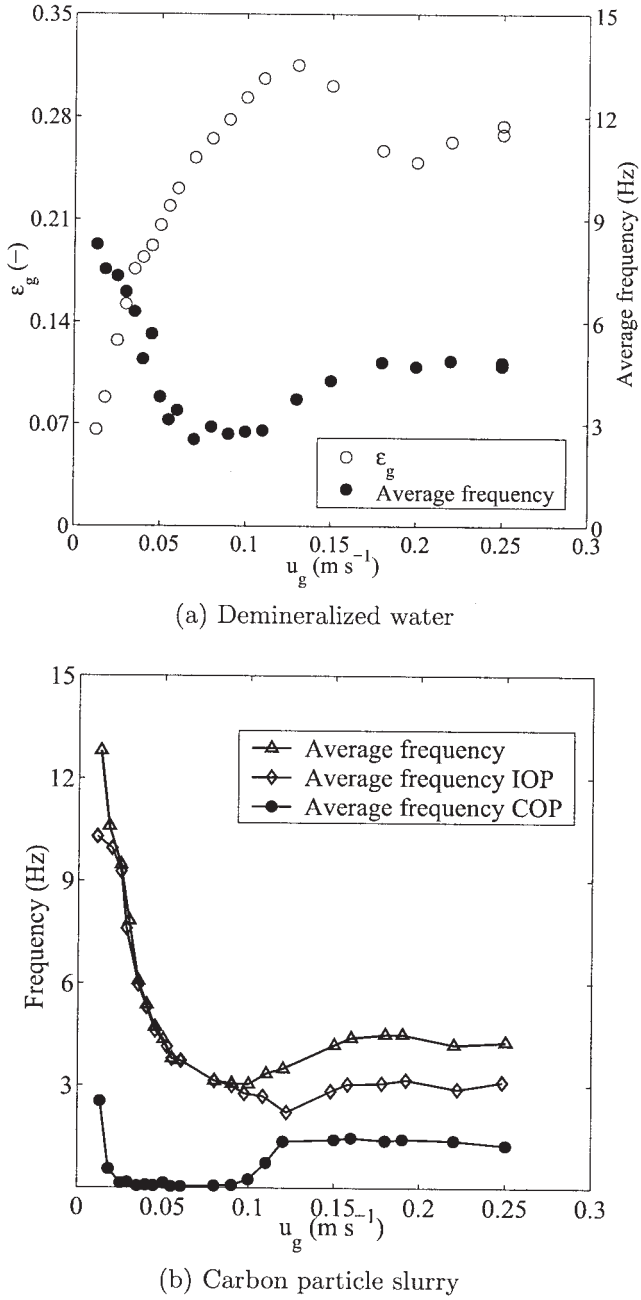

Figure 11. Gas holdup and average frequency of measured pressure time series against superficial gas velocity in a 3-D (slurry)bubble column.

The average frequency of the IOP and COP against gas velocity is also shown using sensor P3.

Heterogeneous regime

In the heterogeneous regime, frequent bubble breakup, bubble coalescence, and violent liquid circulations are observed, which induce rapid gas dispersion. The equilibrium average large bubble diameter is approximately 5 cm, and the frequency of occurrence is 13 bubbles per s (see Figure 9). For all measurement positions, the power in the PSD shows large peaks at frequencies of 2 - 3 Hz, and 6 - 10 Hz (Figures 5a and 5c). Since the amplitudes of these two peaks in the PSD are proportionally increasing, the ratio of the amplitudes is constant. Therefore, the average frequency is approximately constant with a value between 6 and 9 Hz. The two peaks in the PSD are highly coherent and the coherence increases with gas velocity. This means that the coherent sources of pressure waves increasingly dominate the power in the PSD at 2 - 3 Hz

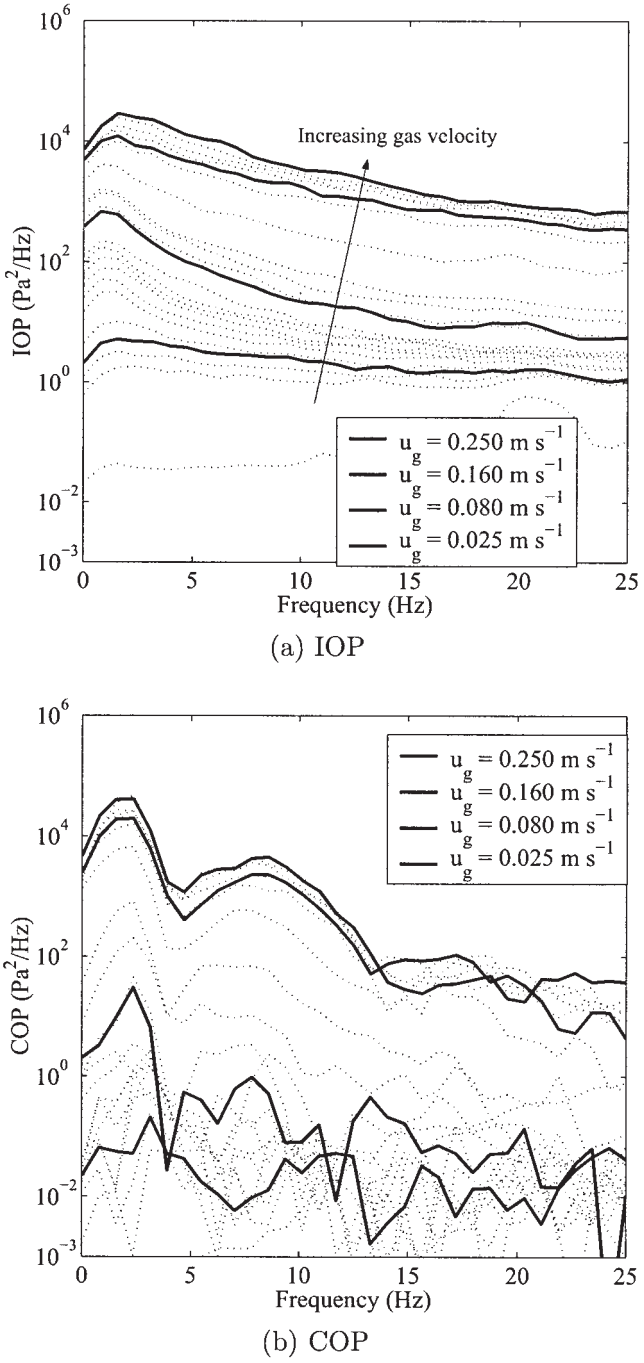

Figure 12. Semilog plot of the incoherent output power (IOP) and the coherent output power (COP) against frequency as a function of superficial gas velocity for 0.5 g l^{-1} carbon particle slurry in a 3-D slurry bubble column.

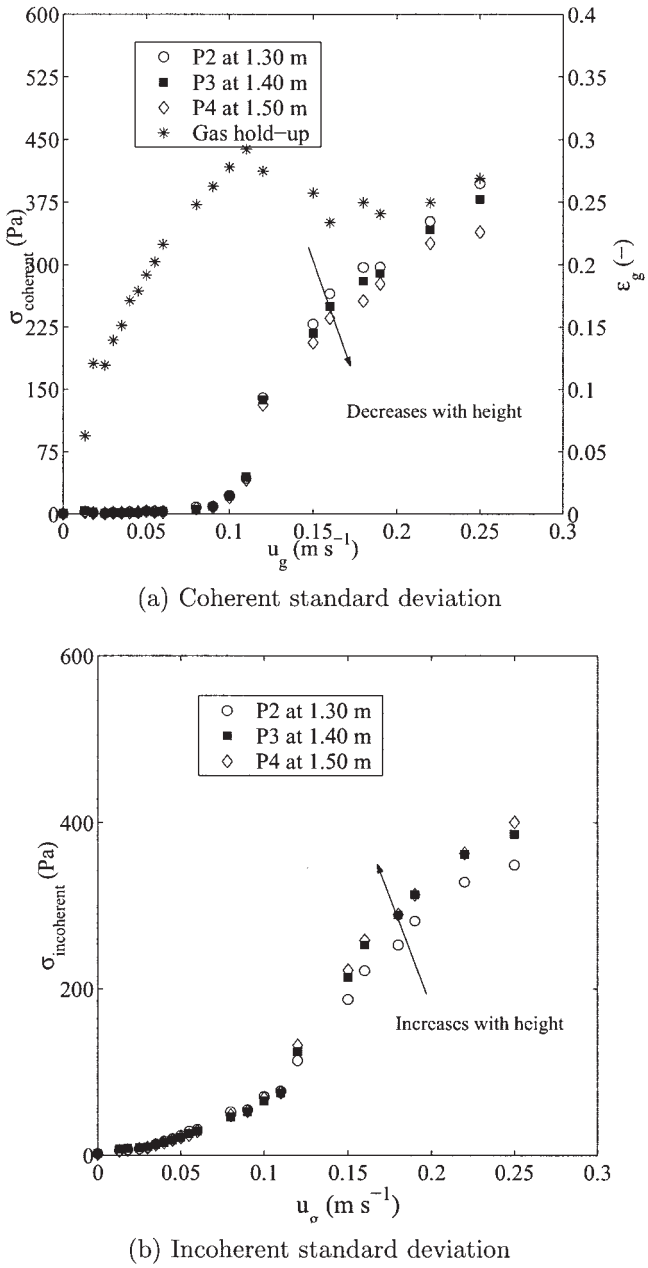

Figure 13. The standard deviation of the incoherent output power (IOP) and coherent output power (COP) against superficial gas velocity for 0.5 g l^{-1} carbon particle slurry in a 3-D slurry bubble column.

At g = 0.09 m s^{-1}, the coherent standard deviation starts increasing, which is referred to as the first transition point.

and 6 - 10 Hz over the incoherent sources. The main difference between IOP (Figure 7a) with its PSD (Figure 5c) is that the coherent peak at 2 – 3 Hz or 6 – 10 Hz is not observed in the IOP, and is present in the COP (Figure 7b). Furthermore, the noise at approximately 0.4 Hz is still present in the IOP. At high gas velocities however, it becomes less dominant. No other peaks are observed in the IOP and the power decreases gradually with increasing frequency.

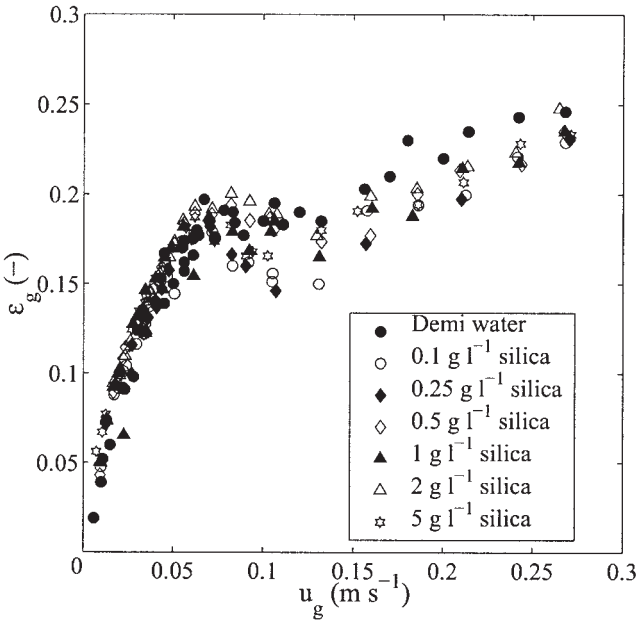

(a) 2D column

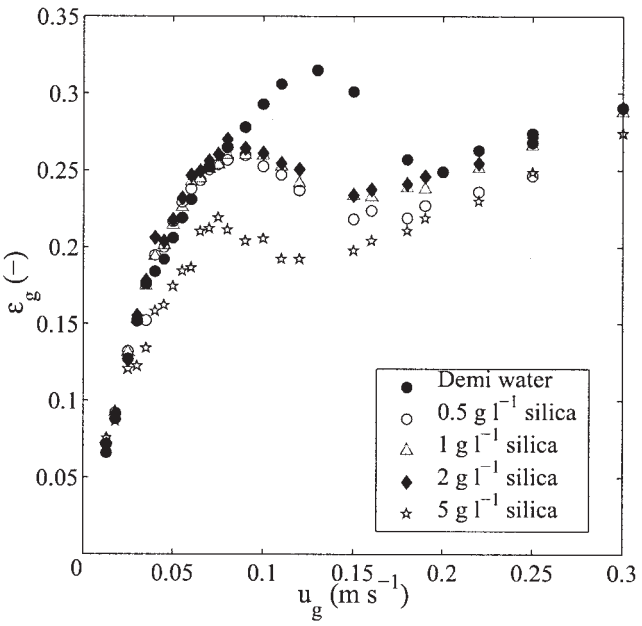

(b) 3D column

Figure 14. Gas hold-up against superficial gas velocity for demineralized water and silica particle concentration in the 2-D and the 3-D slurry bubble column.

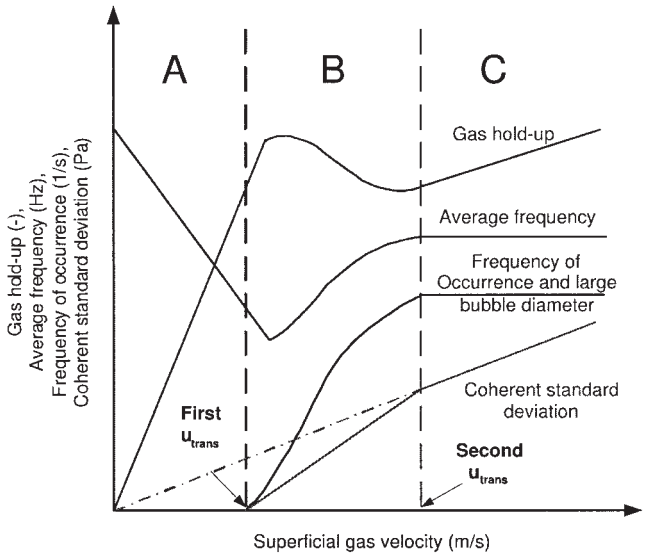

(a) 2D slurry bubble column

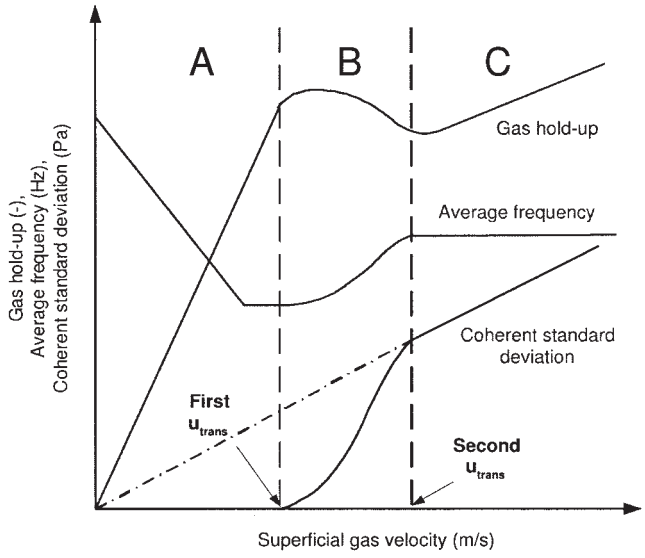

(b) 3D slurry bubble column

Figure 15. Representation of gas holdup, average frequency, frequency of occurrence of large bubbles, and coherent standard deviation against superficial gas velocity in the 2-D and the 3-D slurry bubble columns.

Symbols A, B, and C represents homogeneous regime, transition regime, and heterogeneous regime, respectively.

3-D slurry bubble column

In the 3-D bubble column, the quantification of the large bubble diameter, and its frequency of occurrence is very difficult. Hence, the physical interpretation of the pressure time series in the 2-D column, which has been validated by video image analysis, is also used in the 3-D bubble column.

In the homogeneous regime, the power in the PSD increases with gas velocity over the complete range of frequencies. There is more power in the frequency range of 10 to 20 Hz (Figure 10a). The minimum in the average frequency at u_g = 0.07 m

s^{-1} stays at the same minimum value up to $u_g = 0.10$ m s^{-1} (see Figure 11). This is a remarkable difference between the 2-D and the 3-D bubble columns. Figure 13a shows that the coherent standard deviation is nearly zero till $u_g = 0.09$ m s^{-1}. The point where the coherent standard deviation increases sharply from a zero value is attributed to the first transition point. At this point, the large gas bubbles are formed. Figure 13b shows that the incoherent standard deviation increases slowly till $u_g = 0.09$ m s^{-1}, and afterwards increases sharply.

In the transition regime, the power in the PSD between $u_g = 0.10$ and 0.15 m s^{-1} is significantly different from the power in the PSD in the homogeneous regime. For slurries of carbon and silica particles, the power in the PSD in the frequency ranges of 2 – 3 Hz and 8 – 12 Hz increases steadily as the frequency of occurrence of large bubbles increases. This increases the average frequency up to $u_g = 0.15$ m s^{-1}, beyond which it does not increase further with gas velocity. Figure 13a shows that the coherent standard deviation increases rapidly in this regime upon increasing the gas velocity. The slope of the coherent standard deviation decreases at a gas velocity of 0.15 m s^{-1}. Figure 13b first shows that the incoherent standard deviation does not increase as sharply as coherent standard deviation of pressure fluctuations, and second, the decrease of the slope is not clear. Therefore, the incoherent standard deviation of pressure fluctuations cannot be used for regime transition. The point where the coherent standard deviation changes its slope, and the average frequency becomes constant is attributed to the second transition point, that is, the start of the fully developed heterogeneous regime.

In the heterogeneous regime, the power in the PSD in Figures 10a and 10b shows a strong peak at a characteristic frequency of 2 – 3 Hz and 10 – 12 Hz. Since the amplitudes of these two peaks in the PSD are proportionally increasing, the ratio of amplitudes of power at any two frequencies becomes constant. Therefore, the average frequency remains approximately constant between 4 – 6 Hz. In this regime, the average maximum large bubble diameter predicted by Urseanu[4] reaches approximately 4.5 cm. Summarizing, the coherent standard deviation is sufficiently able to distinguish the two transition points and the three flow regimes in a 3-D slurry bubble column.

For the 2-D and the 3-D slurry bubble column, in the heterogeneous regime, the coherent standard deviation appears to be linearly proportional to the gas velocity without any offset ($\sigma_c \propto u_g$), see Figures 8a and 13a. The magnitude of liquid circulation is also proportional to the gas velocity.[30] This may indicate that the coherent standard deviation is a measure of liquid velocity fluctuations which will be investigated in future studies. Similarly, the incoherent standard deviation of pressure time series can be used as a measure of the large bubble diameter.[35] The average frequency also appears to detect the first and second transition points. However, these transitions do not always correspond to changes in the physical phenomena observed by video imaging. Consequently, the average frequency is less suitable for the detection of transition points.

Conclusions

This article presents a unique and unambiguous flow regime transition identification method, based on the coherent standard deviation and the average frequency of pressure fluctuations in (slurry) bubble columns. The coherent standard deviation of pressure time series, measured at two different locations in the column, is used to separate the global pressure fluctuations that are present throughout the column from the local pressure fluctuations that are directly related to rising large gas bubbles. The coherent standard deviation clearly marks the first and the second transition points. The average frequency can be used to confirm the second transition point. The method of the coherent standard deviation and the average frequency is also applied to pressure time series measured in a 3-D slurry bubble column. The characteristics of flow regimes and regime transitions are shown in Figure 15a for the 2-D, and Figure 15b for the 3-D slurry bubble column:

- In the homogeneous regime, the diameter of the gas bubbles is approximately 4 to 6 mm. Only these small gas bubbles generate pressure fluctuations as they rise upward in the column. In the video, liquid phase circulations and clusters of small bubbles are already observed. The liquid moves upward in the center of the column and downward at the wall. The coherent standard deviation of pressure time series is zero and the average frequency of pressure time series decreases with increasing gas velocity. The gas holdup increases with gas velocity.
- At the first transition point from the homogeneous to the transition regime, the first large bubbles are detected, with a dia. of 1.5 cm, and with a frequency of occurrence of one bubble per s. At this point, the coherent standard deviation of the pressure time series increases from zero.
- In the transition regime, the diameter and the frequency of occurrence of the large gas bubbles increases strongly with increasing gas velocity. The coherent standard deviation of pressure time series increases with increasing gas velocity. The average frequency attains a minimum and then increases with increasing gas velocity. The gas holdup attains a maximum at the minimum point in the average frequency, and then the gas holdup decreases with increasing gas velocity.
- At the second transition point from the transition regime to the heterogeneous regime, the average large bubble diameter and the frequency of occurrence of the large bubbles become constant. At this point, the slope of the coherent standard deviation versus gas velocity decreases and the average frequency becomes constant. The gas holdup against superficial gas velocity attains a local minimum near this point.
- In the heterogeneous regime, the coherent standard deviation increases proportionally with gas velocity, and the average frequency is constant. The gas holdup increases with gas velocity.

Acknowledgment

The authors gratefully acknowledge the Dutch Technology Foundation STW (Project EPC. 5239), Akzo Nobel, DSM Research, Sasol Technology Netherlands, and Shell Global Solutions for their financial support and Engelhard, Norit, and Promeks ASA for supplying the catalyst supports.

Notation

d_b = bubble diameter, m
d_p = diameter of particle, m
f = frequency, Hz
$\bar{f}$ = average frequency, Hz
f_s = sampling frequency, Hz
$\mathcal{F}_x$ = discrete Fourier transform, Pa
n = counter
N = number of frequency components
P = dynamic pressure
$\bar{p}_x$ = average pressure of a pressure time series, Pa
t = time, s
u_g = superficial gas velocity, m s^{-1}

u_{trans} = gas velocity at transition point, m s^{-1}
V_l = liquid volume, m^3
x = referred as position near the sparger in the bubble column, m
y = referred as any position in the bubble column, m

Greek letters

ε_g = volume fraction of gas per unit liquid volume
ε_{trans} = volume fraction of gas bubbles at transition point
ρ_s = density of solid, kg m^{-3}
Φ_{xx} = power spectral density at measurement position x, Pa^2/Hz
Φ_{xy} = cross power spectral density between measurement position x and y, Pa^2/Hz
γ^2_{xy} = coherence between measurement positions x and y, dimensionless
σ = standard deviation, Pa
σ_c = coherent standard deviation, Pa
σ_i = incoherent standard deviation, Pa

Abbreviations

2-D = two-dimensional (flat bubble column)
3-D = three-dimensional (cylindrical bubble column)
COP = coherent output power, Pa^2/Hz
CSD = cross power spectral density, Pa^2/Hz
DFT = discrete Fourier transform
IOP = incoherent output power, Pa^2/Hz
PSD = power spectral density, Pa^2/Hz
SBC = slurry bubble column

Literature Cited

1. Deckwer W-D, Schumpe A. Improved tools for bubble column reactor design and scale-up. *Chem Eng Sci*. 1993;48:889-911.
2. Joshi JB, Parasu Veera U, Prasad CV, Phanikumar DV, Deshpande NS, Thakre SS, Thorat BN. Gas hold-up structure in bubble column reactors. *PINSA*. 1998;64:441-567.
3. Koide K. Design parameters of bubble-column reactors with and without solid suspensions. *J Chem Eng Jpn*. 1996;29:745-759.
4. Urseanu MI. *Scaling up bubble column reactors*. The Netherlands: University of Amsterdam; 2000. PhD Thesis.
5. de Swart JWA, van Vliet RE, Krishna R. Size, structure and dynamics of large bubbles in a 2-dimensional slurry bubble-column. *Chem Eng Sci*.1996;51:4619-4629.
6. Reilly IG, Scott DS, De Bruijn TJW, MacIntyre D. The role of gas phase momentum in determining gas holdup and hydrodynamic flow regimes in bubble column operations. *Can J Chem Eng*. 1994;72:3-12.
7. Wilkinson PM, Spek AP, van Dierendonck LL. Design parameters estimation for scale up of high pressure bubble columns. *AIChE J*. 1992;38:544-554.
8. Boyer C, Duquenne A-M, Wild G. Measuring techniques in gas-liquid and gas-liquid-solid reactors. *Chem Eng Sci.* 57:3185-3215, 2002.
9. Krishna R, Ellenberger J, Maretto C. Flow regime transition in bubble columns. *Int Comm Heat Mass Transfer*. 1999;26:467-475.
10. Lin T-J, Reese J, Hong T, Fan L.-S. Quantitative analysis and computation of two-dimensional bubble columns. *AIChE J.*, 1996;42:301-318.
11. Mudde RF, van den Akker HEA. Dynamic behaviour of the flow field of a bubble column at low to moderate gas fractions. *Chem Eng Sci,* 1999;54:4921-4927.
12. Ruzicka MC, Drahos J, Fialova M, and Thomas MH. Effect of bubble column dimensions on flow regime transition. *Chem. Eng. Sci.,* 56: 6117-6124, 2001.
13. Zahradnik J, Fialova M, Ruzicka MC, Drahos J, Kastanek F. Thomas NH. Duality of gas-liquid flow regimes in bubble column reactors. *Chem Eng Sci*. 1997;52(21-22):3811-3826.
14. Drahos J, Zahradnik J, Puncochar M, Fialova M, Bradka F. Effect of operating conditions on the characteristics of pressure fluctuations in a bubble column. *Chem Eng and Proc*. 1991;29:107-115.
15. Letzel HM, Schouten JC, Krishna R, Van den Bleek CM. Characterization of regimes and regime transitions in bubble-columns by chaos analysis of pressure signals. *Chem Eng Sci*. 1997;52:4447-4459.
16. Vial C. Camarasa E, Poncin S, Wild G, Midoux N, Bouillard J. Study of hydrodynamic behaviour in bubble columns and external loop airlift reactors through analysis of pressure fluctuations. *Chem Eng Sci*. 2000;55:2957-2973.
17. Drahos J, Bradka F, Punchocar M. Fractal behaviour of pressure fluctuation in bubble column. *Chem Eng Sci.* 47:4069-4075, 1992.
18. Fan LT, Neogi D, Yashima M, Nassar R. Stochastic analysis of three phase fluidized bed: Fractal approach. *AIChE J*. 1990;36:1529-1535.
19. Lin T-J, Juang R-C, Chen Y-C, Chen C-C. Predictions of flow transition in a bubble column by chaotic time series analysis of pressure fluctuation signals. *Chem Eng Sci*. 2001;56:1057-1065.
20. Olmos E, Gentric S, Poncin S, and Midoux N. Description of flow regime transitions in bubble columns via laser doppler anemometry signals processing. *Chem Eng Sci.* 2003;58:1731-1742.
21. Vial C, Poncin S. Wild G, Midoux N. A simple method for regime identification and flow characterisation in bubble columns and airlift reactors. *Chem Eng and Proc*. 2001;40:135-151.
22. Bakshi BR, Zhong H, Jiang P, Fan L-S. Analysis of flow in gas-liquid bubble columns using multi-resolution methods. *Trans. Inst. Chem. Eng.,* 1995;73;608-614.
23. Kluytmans JHJ, van Wachem BGM, Kuster BFM, Schouten JC. Gas holdup in a slurry bubble column: Influence of electrolyte and carbon particles. *Ind Eng Chem Res*. 2001;40:5326-5333.
24. Daly JG, Patel SA, Bukur DB. Measurement of gas holdups and sauter mean diameter in bubble column reactors by dgd method. *Chem Eng Sci*. 1992;47:3647.
25. Sriram K, Mann R. Dynamic gas disengagement: a new technique for assessing the behaviour of bubble columns. *Chem Eng Sci.* 1977;32: 571-580.
26. Krishna R, Sie ST. Design and scale-up of the fischer-tropsch bubble-column slurry reactor. *Fuel Process Technol*. 2000;64:73-105.
27. Richardson JF, Zaki WN. Sedimentation and fluidisation: Part 1. *Trans Instn Chem. Engrs*. 1954;32:35.
28. Ruzicka MC, Zahradnik J, Drahos J, Thomas NH. Homogeneous heterogeneous regime transition in bubble columns. *Chem Eng Sci*. 2001;56:4609-4626.
29. Wallis GB. One-dimensional two phase flow. McGraw-Hill, New York; 1969.
30. Zuber N, Findlay JA. Average volumetric concentration in two-phase flow systems. *J Heat Transfer, ASME* 1965;87:453-468.
31. J Drahos. Quo vadis, the analysis of time series in reactor engineering? *Trans Inst Chem Eng*. 2003;81(A):411-412.
32. Gluszek J, Marcinkowski R. Pressure oscillations in bubble columns. *Chem Eng J*. 1983;26:181.
33. Lamb H. Surface waves. In Hydrodynamics, book chapter IX, page 364. New York: Cambridge University Press; MacMillan Co. 1945.
34. Mallock A. Absorption of sound by gas bubbles in liquids. *Proc Roy Soc London*, 1910;84:39.
35. Chilekar VP, Warnier MJF, van der Schaaf J, van Ommen JR, Kuster BFM, Schouten JC. Bubble size estimation in slurry bubble columns from pressure fluctuations. *AIChE J*. in press 2005.
36. van der Schaaf J, Schouten JC, Johnsson F, van den Bleek CM. Non-intrusive determination of bubble and slug length scales in fluidized beds by decomposition of the power spectral density of pressure time series. *Int J Multiphase Flow*, 2002;28:865-880.
37. Randall RB. *Frequency analysis*. 3rd ed. Denmark: Bruel and Kjaer; 1987.
38. Jenkins GM, Watts DG. *Spectral analysis and its applications*. San Francisco: Holden Day; 1968.
39. Kluytmans JHJ. *An airlift loop redox cycle reactor for alcohol oxidations: Hydrodynamics, mass transfer and reactor design*. The Netherlands: Eindhoven University of Technology; 2003. PhD Thesis.
40. Krishna R, Urseanu MI, van Baten JM, Ellenberger J. Rise velocity of a swarm of large gas bubbles in liquids. *Chem Eng Sci*. 1999;54:171-183.
41. Lapin A, Lubbert A. Numerical simulation of the dynamics of two-phase gas-liquid flows in bubble columns. *Chem Eng Sci.* 1994;49:3661-3674.

Manuscript received July 19, 2004, and revision received Dec. 1, 2004.